



Analysis of the development of drainage basins during active fold growth (Chenareh anticline, Zagros fold-and-thrust belt, Iran)

Somaye Derikvand *

College of Sciences, Lorestan University, Khoramabad, 68148, Iran

Received: 10 March 2024, Revised: 02 June 2024, Accepted: 28 July 2024

© University of Tehran

Abstract

Fold-and-thrust belts (FTBs) have widely developed in active orogenic systems. As structural shortening accumulates, thrust-related folding can increase in amplitude and length, causing progressive tectono-morphologic evolution of the FTB. I analyzed the growth of folds in the Chenareh anticline in southern Lorestan Province (Zagros FTB, Iran). I focus on tectonic geomorphological criteria for detecting the lateral growth of folding in tectonically active settings because of their relative ease and low cost. Due to the variety of drainage basins and their networks along the axis of the anticline as well as transversely across its forelimb and backlimb, the Chenareh anticline was considered suitable for applying morphometric indices. The morphometric characteristics of the 108 drainage basins in the study area were analyzed. The main drainage sinuosity (Smd), sinuosity of the anticline divide (Sd), and crescentness index (CI) parameters are greater, and the asymmetry factor (AF), hypsometric integral (HI), basin shape (Bs), drainage frequency (Df), drainage density (Dd), drainage density of 1st-order streams (Dd1), and ratio of streams of order 1 to the total number of streams (N1/N) are lower in the central zone than in the eastern and western fold plunge zones. The changes in these parameters correspond to the lateral growth of the fold from the center to the eastern and western fold noses. Structural and geomorphological observations confirm the results of quantitative geomorphological indices as reliable evidence of the propagation of lateral folds. Our evidence indicates the lateral growth of folds in the western and eastern zones of the anticline.

Keywords: Tectonic Geomorphological Indices, Drainage Basin, Anticline, Active Tectonics

Introduction

Active deformation during fold-and-thrust belt (FTB) development has the potential to trigger destructive earthquakes (e.g., Hubbard and Shaw, 2009; Xu et al., 2009; Lu et al., 2017). The growth of thrusts and folds shifts convective and horizontal rock masses, which controls the evolution of drainage networks and topographic slopes (e.g., Bufe et al., 2016; Bahrami et al., 2020). Accordingly, research on the active tectonics of FTBs has critical implications for the assessment of geological hazards and environmental changes. Active orogenic belts show different geomorphic features as a result of both exogenic and endogenic processes.

Active tectonics have been widely studied using various geomorphic indices because of their ability to detect landscape responses to tectonic drivers (e.g., Lavé and Avouac, 2000; Keller and Pinter, 2002; Zielke et al., 2010). The results of measured indices help to evaluate the relative roles of variations in rock resistance and crustal displacement during landscape

* Corresponding author e-mail: derikvand.so@lu.ac.ir

development (e.g., Walcott and Summerfield, 2008). In addition, understanding the structural and tectonic style of fold-thrust belts as hydrocarbon traps is a significant challenge in the petroleum industry. Tectonic geomorphological analysis can reveal the linkage pattern and history of fold growth (Zarei et al., 2023).

Fluvial courses are interpreted as indicators of fold propagation due to the lateral growth of anticlines and fan-shaped branching patterns on fold flanks and other geomorphological features (such as water gaps and wind gaps) (Ramsey et al., 2008). Typical geomorphic evidence of fold lateral growth in the FTB includes the following (Keller et al., 1999; Ramsey et al., 2008; Bretis et al., 2011; Sissakian et al., 2019; Machuca et al., 2021; Adeoti and Webb, 2022; Bahrami and Stoke, 2023): 1) the development of asymmetric drainage patterns; 2) a decrease in the drainage density and degree of dissection; 3) a reduction in the relief and height of wind gaps along the topographic profile parallel to the folding hinge line; 4) the deformation of progressively younger landforms or deposits; 5) the creation of curved wind gaps; 6) a reduction in the rotation and inclination of fold limbs; and 7) the creation of fan-shaped tributary drainage patterns on the flanks of folds.

The Alpin-Himalayan orogenic system is formed by complex geomorphic and geological processes (Mukherjee et al., 2013; Mukherjee, 2015). The Zagros FTB is one of the best examples of active orogeny in this orogenic system, which results from deformation related to the Neogene continental collision of the Arabian plate with the Eurasian continent. However, the tectonics of the Zagros are not fully understood. This belt contains prominent "whale-back" anticlines that grow vertically and laterally (Ramsey et al., 2008; Collignon et al., 2016; Woodbridge et al., 2019). Several studies have focused on the morphometry and development of drainage systems (Mumipour et al., 2011; Alipoor et al., 2011; Al-Saady et al., 2016; Zarei et al., 2024), while geomorphological evidence of vertical and lateral fold growth in the Zagros FTB has been less evaluated. Researchers have studied river-folding interactions in some areas of the Zagros River (Bahrami, 2013; Burberry et al., 2008; Ramsey et al., 2008; Walker et al., 2011; Obaid and Allen, 2017;). Although the southern parts of the Zagros belt have been studied in detail (Bahrami et al., 2020; Zarei et al., 2023; Bahrami and Stokes, 2023), the northern parts have received considerably less attention.

Geomorphic quantitative analysis of landscapes and landform components using satellite images and digital elevation models (DEMs) is a low-cost method with relatively simple operations. The Chenareh anticline (CH-Ant) is considered appropriate for the use of morphometric indices in drainage basins (i.e., asymmetry, circularity, elongation, crescentness index, and hypsometric integral) and river networks (i.e., frequency and drainage density) that develop along the axis of the anticline and transversely across its forelimb and backlimb. This paper investigates the morphometry of basins and drainage networks to analyze the active tectonics and lateral growth of the CH-Ant in the Zagros orogenic belt.

For this purpose, regional landscape responses to potential tectonic activity were studied using geomorphic parameters (asymmetry factor (AF), hypsometric integral (HI), basin shape (Bs), crescentness index (CI), main drainage sinuosity (Smd), sinuosity of anticline divide (Sd), drainage frequency (Df), drainage density (Dd), and the ratio of streams of order 1 to the total number of streams (N1/N)).

Study area

Geological features

The Chenareh anticline (CH-Ant) is located in the central part of the Zagros FTB. The Zagros FTB is situated in the southwestern part of Iran and has a northwest–southeast trend (Fig. 1a). The Zagros orogenic belt is 1800 km long and extends from Mount Taurus in northern Turkey to

the Strait of Hormuz in Iran (Alavi, 1994). This belt was created during the continental collision between the Arabian and Eurasian plates in the Tertiary period (Agard et al., 2005). The total percentage of bulk shortening in the Zagros belt is approximately 30-32% (Bahroudi and Koyi, 2003). Based on earthquake seismicity and GPS analysis, present-day plate movements indicate north–northeast movement of the Arabian plate into the Eurasian plate at a rate of approximately 25–30 mm/yr (Talebian and Jackson, 2002). GPS analyses indicate N ~ 5°E movement at 25 mm/yr for the Arabian plate toward southwest Iran (McClusky et al., 2003).

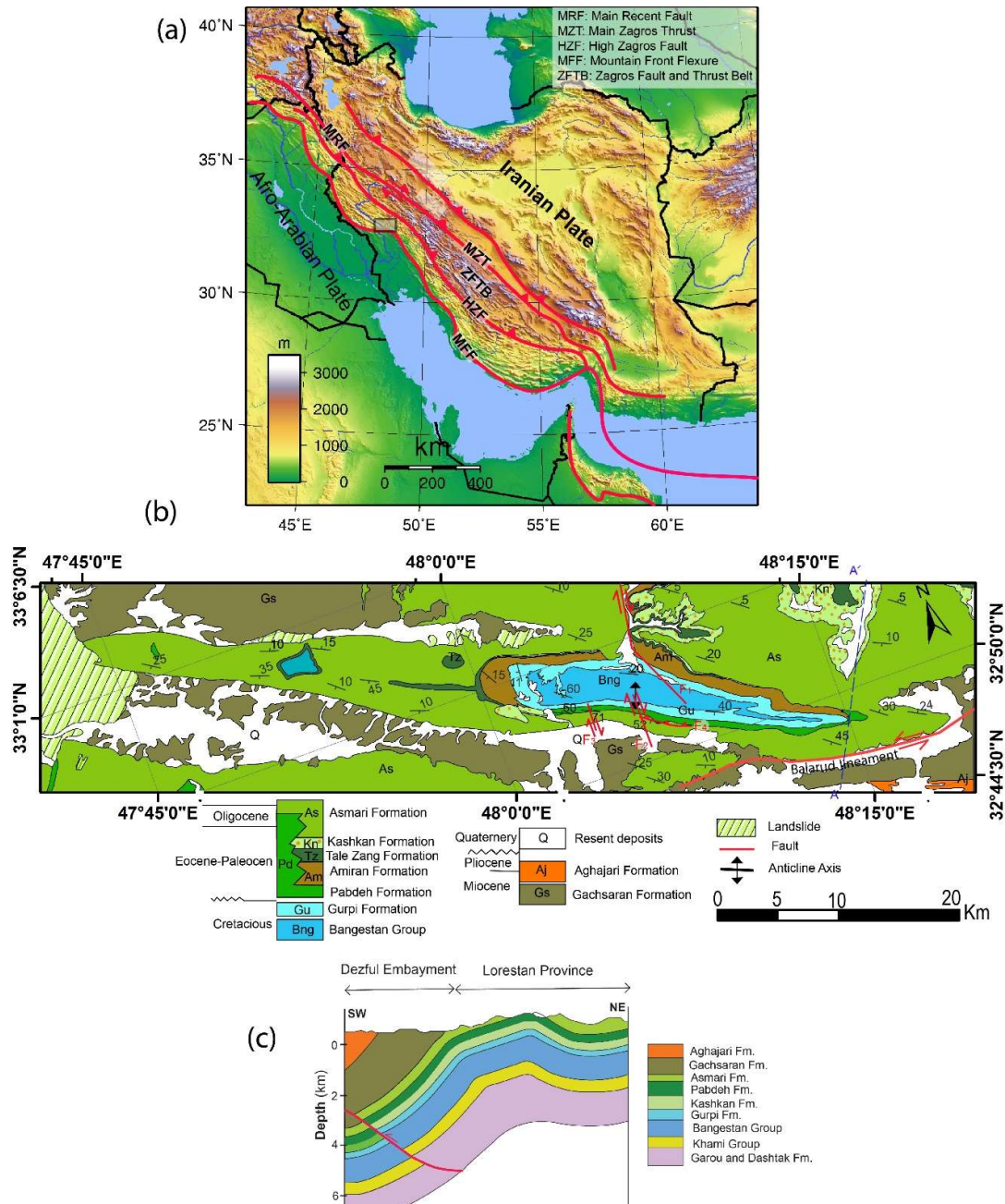


Figure 1. a) Iran digital elevation map. The orogenic belt of Zagros is located in western Iran (Alavi, 1994). The black rectangle and the red lines show the study area and the main faults, respectively. b) Geological map of the study area at a scale of 1:100,000 (National Iranian Oil Company) showing the location of the constructed cross section AA'. c) Cross section AA' across the anticline is oriented NE–SW (prepared from a structural-geological map)

This convergence occurs $\sim 50^\circ$ oblique to the dominant NW–SE strike of the central Zagros FTB (McClay et al., 2004). As a result of this convergence, folds, thrust faults, and large-scale strike-slip faults have formed in the Zagros belt and are still growing and active today (Sarkarinejad and Goftari 2019). The dynamics of this convergence control the topography, landforms, structures, distribution of earthquakes, and active faults in the Zagros belt (Agard et al., 2011). The Zagros foreland orogenic belt is divided into different tectonic zones based on its stratigraphic successions and structural patterns: 1) the Lorestan Province (western Zagros); 2) the Dezful Embayment and Izeh (central Zagros); and 3) the Fars Province (eastern Zagros) (Falcon 1974). The Lorestan Province has well-preserved anticlines from Mesozoic to Neogene carbonate rocks (e.g., Carruba et al., 2006). The CH-Ant fault-related fold is located in the Lorestan Province (Fig. 1).

The outcrops of geological formations in the CH-Ant are from the Middle Cretaceous to the Miocene, while the newer deposits, from the Miocene to the present, form the geological bedrock of the valleys. The oldest geological formation is the Bangestan Group, which has a thick carbonate unit consisting of shale and sandstone (Elyasi et al., 2014). The Gurpi Formation above the Bangestan Group is composed of shale, marl, and marl limestone (Elyasi and Goshtasbi, 2015). In the frontal limb is the Pabdeh Formation (including marl limestone), which laterally turns into the Amiran (including siltstone and sandstone), Taleh Zang (including limestone deposits), and Kashkan (including destructive flash) Formations toward the backlimb. The main and widest outcrop in this anticline is the Asmari Formation (including mainly limestone deposits). Gachsaran (anhydrite, halite, marl, and limestone) and Aghajari (sandstone, marl, gypsum, siltstone) are the youngest Formations. A geological map of the study area is shown in Fig. 1b. A cross-section of AA' was prepared across CH-Ant (Fig. 1c).

Tectonic-geomorphic features

Stratigraphic and tectonic settings control the physiography of the Zagros FTB (Borne and Twidale, 2011). The drainage network is highly compatible with the growth of fold and thrust structures and the erosion of outcrop formations. Due to strain partitioning between the Zagros FTB and the main recent strike-slip fault in the NW of the range (Talebian and Jackson, 2002), the regional plate convergence is approximately N–S (e.g., Vernant et al., 2004). The Balarud fault (BRF) is a segment of the mountain front flexure (MFF) and the boundary between the Dezful subsidence zone and the Lorestan Province (Figs. 1a and 2).

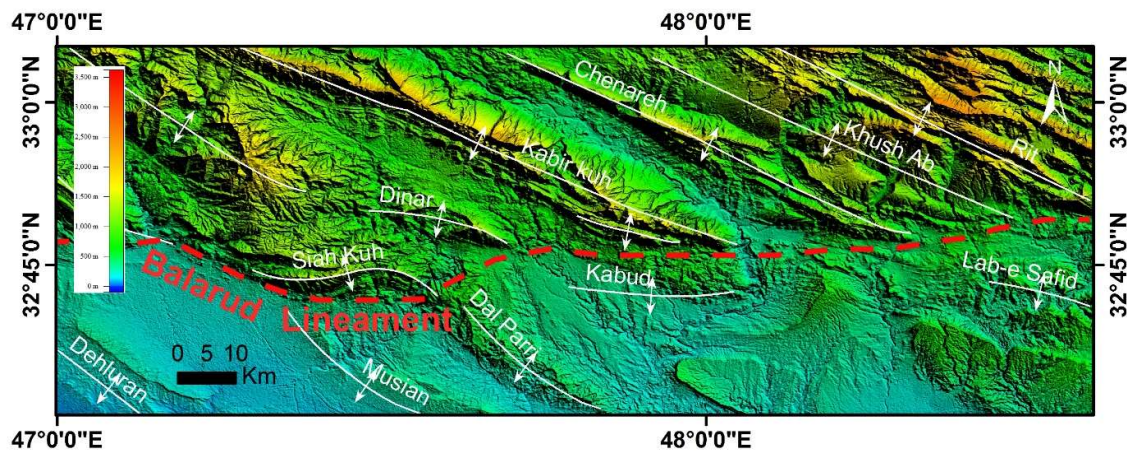


Figure 2. SRTM topography of the Balarud lineament, at the southern side of the Lorestan Province. Anticlines near the Balarud lineament are deflected to more E–W orientations

The BRF plays an important role in the deflection of the surrounding anticlines (Allen and Talebian, 2011) and exerts high control on the tips of folds to either side of it. The Balarud and Kobud anticlines on the southern side have an almost east–west orientation (Fig. 2). CH-Ant plunges and dies out in the vicinity of the BRF lineament. The inverted blind basement BRF plays a significant role in the deformation style of the overlying sedimentary rocks in the study area (Razavi Pash et al., 2021). The CH-Ant lies northwest of the BRF as a left-lateral strike-slip fault with a reverse component. The BRF lineament creates an en-echelon structure and curved axis in the CH-Ant. The CH-Ant trend (NW–SE) changes to an E–W trend in the vicinity of the BRF and shows small sinistral motion.

During different stages of progressive deformation, multiple detachment surfaces and their associated thrust faults have complicated the geometry of thrust-related folds. Figure (3a) shows thrust faults in the Asmari Formation. Thrust-related folding has occurred in the hanging wall of the fault. The CH-Ant appears as a box fold structure due to the morphology of the whale-back. The CH-Ant is a doubly plunging fold with different topographic slopes in its eastern, western, and central parts. Accordingly, CH-Ant is divided into three tectonic zones: eastern, central, and western (Fig. 4). Parallel and consequent drainages are created in the western zone. The flow path is affected by the fractures related to the anticline and the BRF lineament (Fig. 5b). In the central part, the drainage networks are roughly parallel to the hinge of the fold (Fig. 4), and the water gaps cross through the anticline (Fig. 5b). In the studied area, the Zal and Balarod Rivers pass through meandering channels affected by CH-Ant tectonic activity (Fig. 3b).

Lateral fold growth is preserved at the eastern and western tips of CH-Ant with high relief, where wind gaps exist along the fold crest (Figs. 4, 6a, and b). The northeast-dipping fold limb (backlimb) varies between 5 and 25 degrees, while the southwest-dipping fold limb (frontal limb) varies between 50 and 70 degrees. The mutual interaction of the tectonic activity and the erosion processes of the anticline and the dissection of the drainage network caused the formation of steep triangular facets along CH-Ant (Figs. 5, 4c, and d). Wine-glass valleys form as individual valleys by the erosion of triangular facets (Figs. 3c, d, 6c, and d). These valleys indicate recent uplift activities in the region. Narrow and deep gorges (Fig. 6, f and g) near the mountain front delineate the alluvial fans and are another indicator of current active tectonics. Some of the gorges are places where water passes, and some of them are dry valleys. The presence of deep fluvial incisions is confirmed by V-shaped hanging valleys (Fig. 6h), fault scarps, and knickpoints (Fig. 6i and j), indicating tectonic activity in the study area. Well-developed fan-shaped tributary patterns are observed on the flanks of the fold and throughgoing gorges in the Asmari Formation (Fig. 5a and c).

Materials and methods

To evaluate the lateral growth of CH-Ant, ALOS DEM data with a spatial resolution of 12.5 m were used for integrated morphometric techniques and geomorphic data analysis. The length and number of stream orders were calculated. River networks of the study area were extracted through the hydrology toolbox in ArcGIS. Based on Google Earth™ images and ALOS DEM data, 108 drainage basins were identified in the CH-Ant. The midline of the basins was estimated using the distance calculation function in the ILWIS software. The lithology units were extracted from geological maps at a scale of 1:100,000.

The strength of bedrock has a great influence on the morphology and morphometry of drainage networks and landforms (e.g., Nag and Chakraborty, 2003; Stokes and Mather, 2015). The exposure of lithological units with different strengths in the CH-Ant can affect the morphometry of basins and their networks. According to the importance of rock resistance to the morphometry of landforms (Stokes and Mather, 2015), the Formations in the study area can

be divided into three general groups (Sepehr and Honarmandnejad, 2012; Peyrowan and Shariatjafari, 2013).

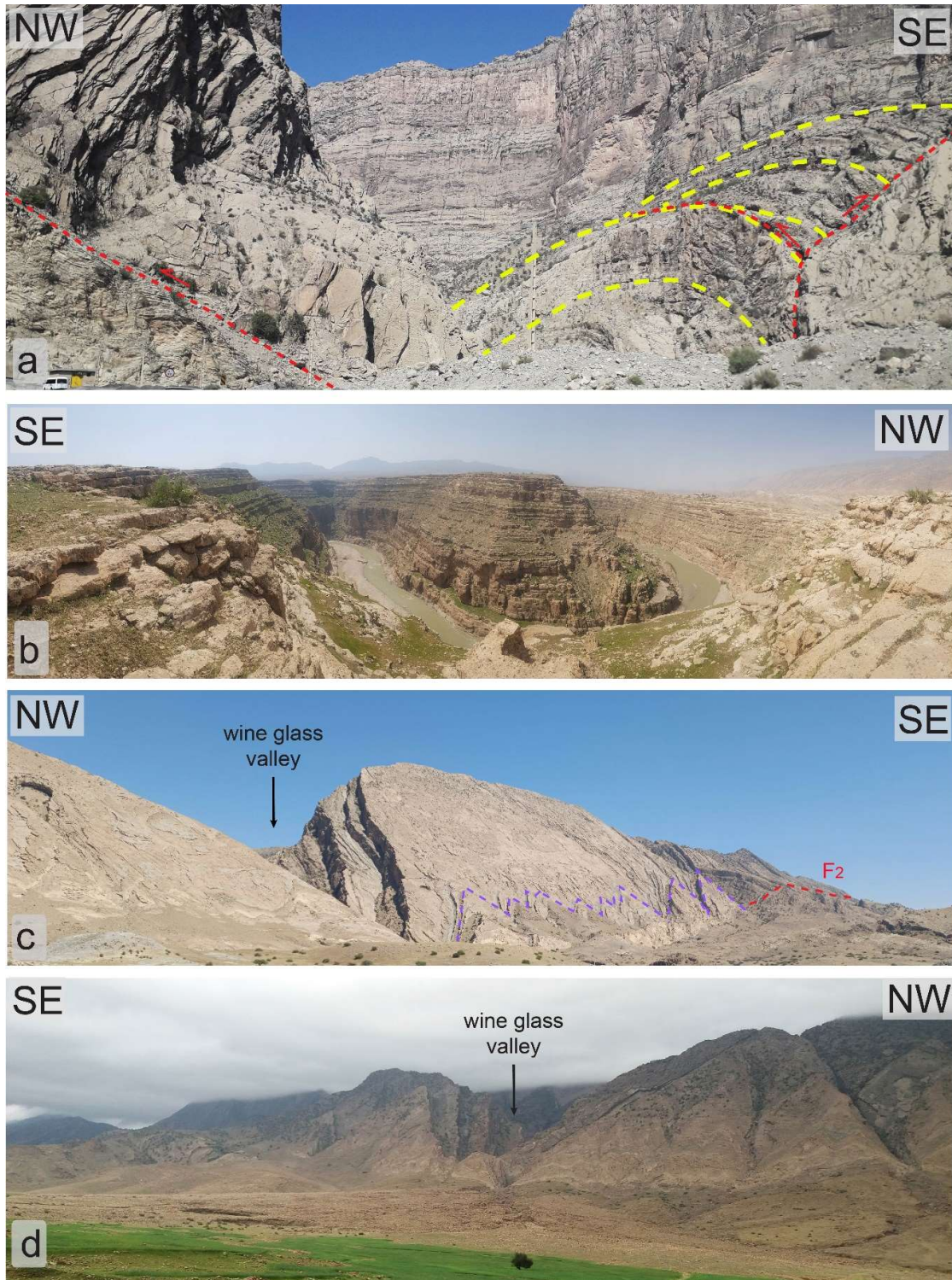


Figure 3. a) Thrust faults in the Asmari Formation are shown with red dashed lines. b) The meandering channel of the Zal River in the central zone. c and d) Triangular faces and wine-glass valleys created in the carbonate rocks of the Asmari Formation. The red dashed line shows the location of the F₂ fault. The blue dashed line shows the border of the triangular facets

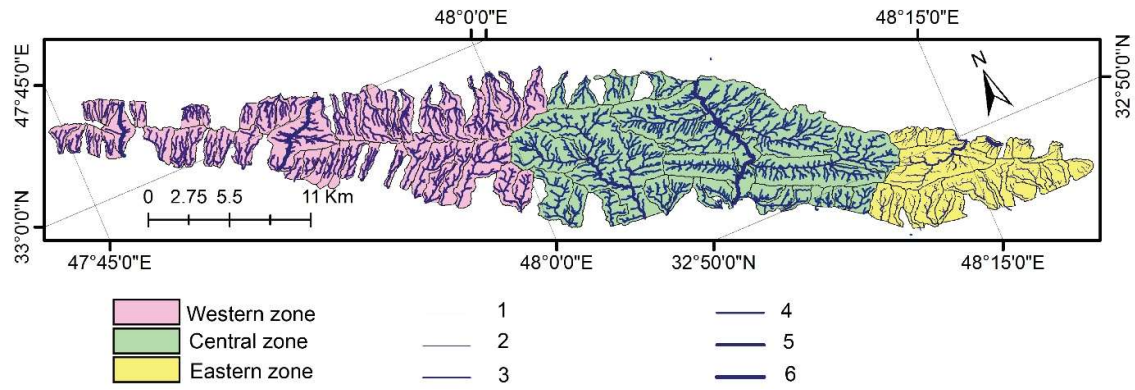


Figure 4. Drainage map of the Chenareh anticline and zonation of its folding structure

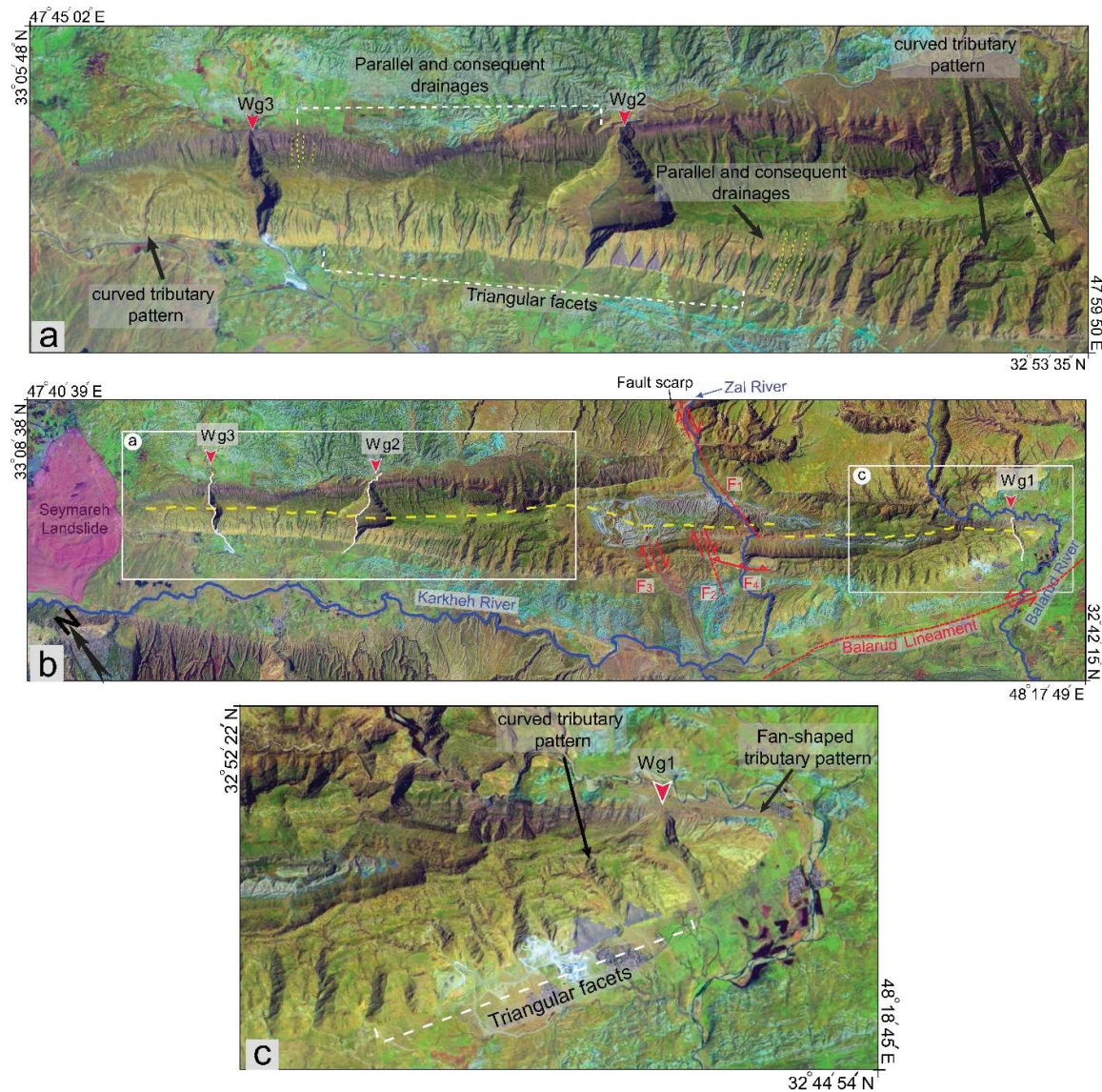


Figure 5. a) Landsat OLI image of the western zone of the Chenareh anticline; the location is given in part (b). b) Landsat OLI image of CH-Ant. c) Landsat OLI image of the eastern zone of CH-Ant; the location is given in part (a)

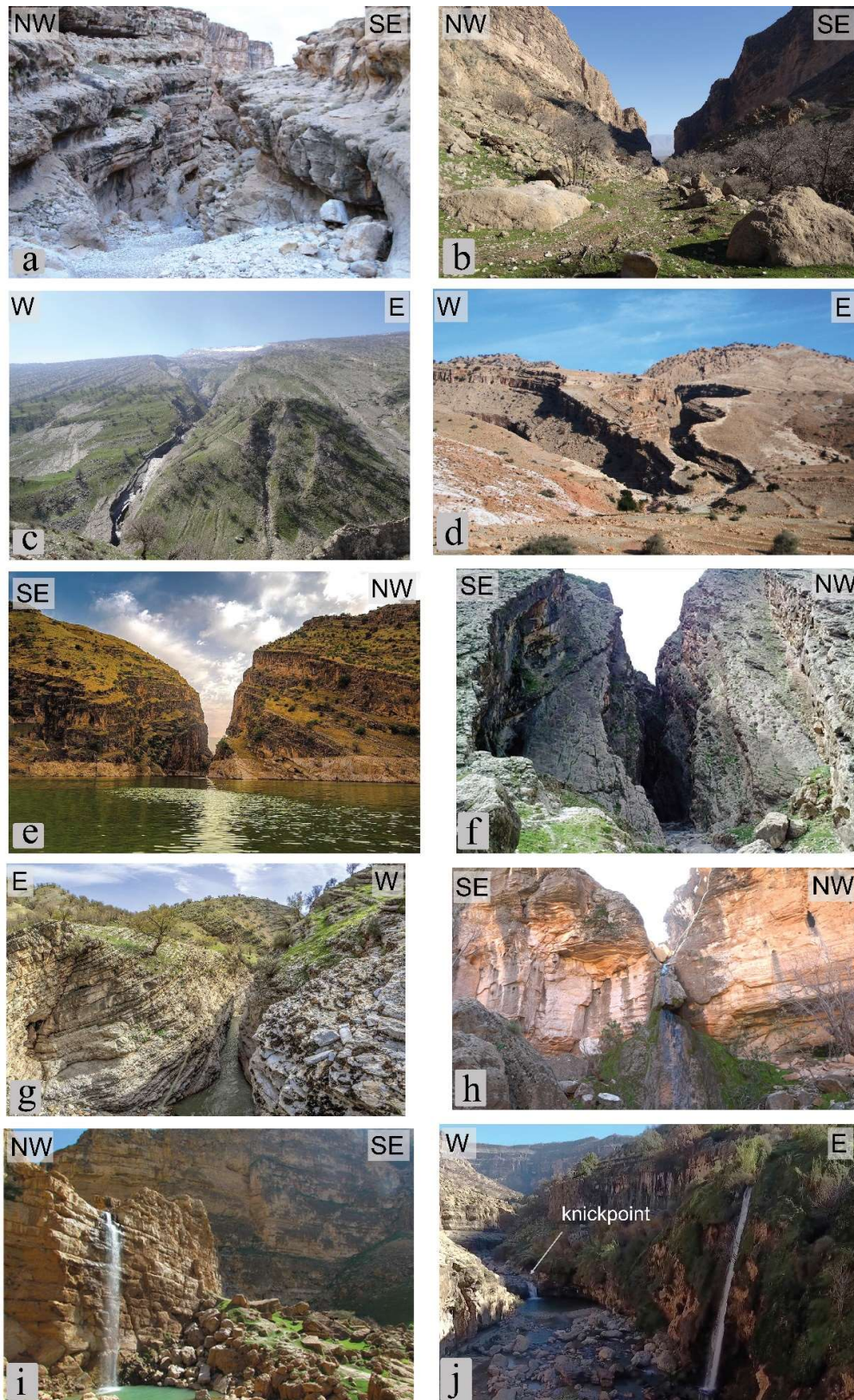


Figure 6. a and b) Images of wind gaps along the fold to the south of the Balarud River. c and d) Wine-glass valleys in the Chenareh anticline. e, f, and g) Deep narrow gorges in the CH-Ant. h) Hanging valley as a tributary valley into the larger valley in the western zone. i and j) Fault scarp features are exposed as knickpoints

Type 1 (strong): Bangestan Group, Taleh Zang, and Asmari Formations. Type 2 (intermediate): Gurpi, Amiran, Pabdeh, Kashkan, Gachsaran, and Aghajari Formations. Type 3 (weak): Quaternary alluvial terraces and deposits. A total of 73%, 18% and 9% of the studied area has strong, intermediate, and weak rock strength, respectively (Fig. 7).

Morphometric indices

Asymmetry factor (AF)

The asymmetry factor (AF) is commonly used to detect tectonic tilting at the drainage basin scale (Keller and Pinter, 2002). The AF is estimated by the following formula (Keller and Pinter, 2002):

$$AF = (A_r / A_t) \times 100$$

Where A_r is the area of the right downstream basin and A_t is the total area of the basin. AF values above or below 50 indicate lithological control, differential erosion, or active tectonics, while AF values close to 50 indicate tectonic stability or no tilting perpendicular to the main trunk channel direction (Pérez-Peña et al., 2010).

Hypsometric integral (HI)

Nondimensional measurements of hypsometric curves and hypsometric integrals (HIs) are useful geomorphic indicators for determining the stages of drainage basin development (Strahler, 1952). The hypsometric curve represents different types of landforms (Strahler, 1952) and is used to study the influence of various factors, such as climate, lithology, and tectonics, on the evolution of landforms. The HI is the area under the hypsometric curve. A second-order polynomial equation was fitted to the hypsometric curve, and then the fitting equation was integrated over the desired ranges (0 to 1) to estimate the HI (Liffner et al., 2018), although the hypsometric integral is generally calculated by the height-to-relief ratio (Pavano et al., 2018). In contrast, low HI values indicate older landscape topography that was more recently eroded but less affected by tectonic activity (He et al., 2019).

Drainage basin shape index (Bs)

In an active tectonic area, the basin shows an elongated shape and becomes circular with topographic evolution or a decrease in tectonic activity (Ramkumar et al., 2019).

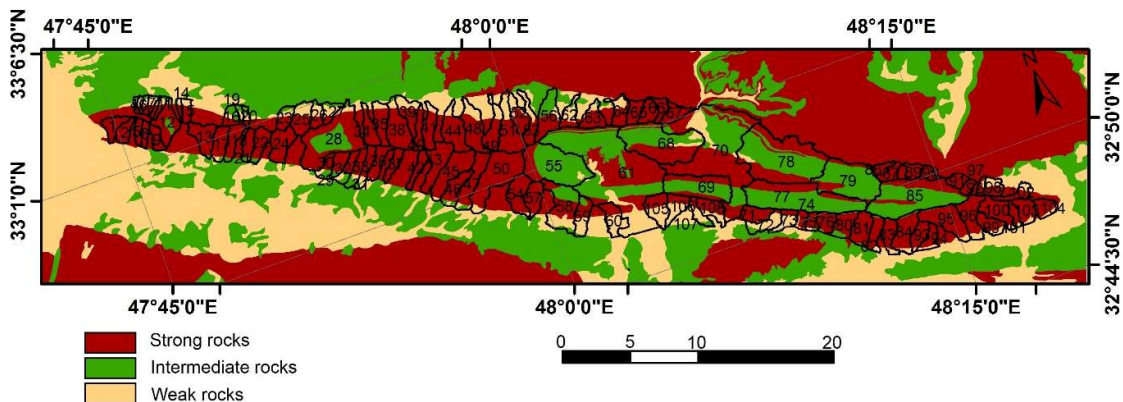


Figure 7. Spatial distribution map of rocks of three strength types: strong, intermediate and weak

The B_s is expressed by the relation $B_s = B_l / B_w$

Where B_l represents the length of the midline basin and B_w represents the width at its widest point (Ramírez-Herrera, 1998). As the folds gradually grow over time, the shape of the basins becomes more circular due to the lateral development of the drainage basins (Bahrami et al., 2020).

Crescentness index (CI)

The crescentness index (CI) is used to correlate the shape of the basins with the vertical and lateral growth of the anticline. This geomorphic index is expressed by (Bahrami et al., 2020):

$$CI = LBM / SL$$

Where LBM is the length of the midline of the basin and SL is the length of the straight line between the ends of the midline of the basin. Low CI values (close to 1) indicate straight basins, while high CI values (close to 1.5) indicate fully crescent basins. Drainage basins that form on fold limbs have higher CI values, which are considered evidence for the development of lateral folds.

Main drainage sinuosity (Smd)

The slope gradient and uplift can affect channel sinuosity. The main drainage sinuosity (Smd) of the basin represents the ratio of the length of the main channel (M_c) to the length of the straight line between the endpoints of the main channel (SL). The sinuosity of the channel is greater in the older and uplifted parts of the anticline channel than in the younger parts (noses) with less erosion (Bahrami and Stokes, 2023).

Sinuosity of the anticline divide (Sd)

The sinuosity of the anticline divide (Sd), as a quantitative index, is defined as

$$Sd = LD / LH$$

Where LD indicates the length of the main divide of the anticline and LH indicates the length of the hinge (Bahrami et al., 2020). In general, lower Sd values correspond to younger, less eroded segments (noses), while higher Sd values correspond to older, more eroded segments of the anticline (core).

Drainage system morphometry

The drainage texture can be determined by the drainage frequency (Df) and drainage density (Dd) of a basin. Drainage frequency and density are generally related to various parameters, such as vegetation, climate, time, surface slope, tectonic uplift, and lithology (Keller and Pinter, 2002; Devi et al., 2011; Bahrami, 2022). Drainage frequency and density can reveal insights from the rates of lateral propagation and uplift of anticlines (Azor et al., 2002; Melosh and Keller, 2013; Bahrami and Stokes, 2023). The drainage frequency represents the total number of stream segments of all orders per unit area, while the drainage density is the ratio of the accumulated total channel lengths for all orders in a basin to the basin area (Horton, 1932). Among drainage orders, first-order drainage is most sensitive to active tectonics (Keller and Pinter, 2002). Hence, laterally growing anticlines have greater N_1/N ratios (Melosh and Keller, 2013; Bahrami, 2022). N_1/N is the ratio of streams of order 1 to the total number of streams of all orders. The Dd, Df, and N_1/N of the main streams in the study area were calculated.

Results

According to the morphometric characteristics, 108 drainage basins have been identified in the anticline of the studied area. The CH-Ant is divided into 3 (western, central, and eastern zones) and 2 (northern and southern zones) tectonic zones with E–W and N–S trends, respectively. The mean values of the morphometric characteristics of the drainage basin (AF, Bs, CI, HI, and Smd), the values of the morphometric properties of the drainage networks (Dd, Dd1, Df, and N1/N), and the sinuosity of the anticline divide (Sd) are summarized in Tables 1 and 2. Based on the values of the AF, HI, Bs, Smd, and CI indices, the basins are classified into three categories: class 1, class 2 and class 3 (El-Hamdouni et al., 2008; Bahrami et al., 2024). Classes 1, 2, and 3 represent high, moderate, and low tectonic activity levels, respectively. Figure (8) shows the results of the zoning map obtained from the results obtained from these parameters.

The area of the drainage basin varies from 0.316 km² (basin 3 in the western zone) to 29.42 km² (basin 61 in the central area). In general, basins with larger areas are located in the central zone. Basin 34 and basin 2 have the highest (85) and lowest (24) topographic slopes, respectively. The lowest HI value (0.41) corresponded to basin 40 (eastern region), and the highest HI value (0.77) corresponded to basin 17 (western region). The longest and most circular basins are basins 2 and 4, respectively. The lowest value of the asymmetry factor (0.81%) is related to basin 31 (central zone), and the highest value (35.2%) is associated with basin 22 (western zone). The mean Bs values are 2.24, 2.16, and 3.24 in the eastern, central, and western zones, respectively. These results show that the western zone has relatively elongated basins compared to the more circular basins in the eastern and central zones. The higher mean values of HI in the western zone (1.04) compared to those in the eastern and central zones (0.52 and 0.49, respectively) show that the basins in the western zone have a younger topography than the other zones. The mean crescent index (CI) is greater in the central zone (1.46) than in the eastern and western zones (1.005 and 1.003, respectively). The main drainage sinuosity (Smd) in the central zone (1.22) is greater than that in the eastern and western zones (1.17 and 1.06, respectively).

Table 1. Mean values of morphometric parameters of 108 basins in three anticline zones. Basins 81 to 104 are in the eastern zone, basins 55, and 58 to 80 are in the central zone, and basins 1 to 54, and 56 and 57 are in the western zone. N represents the number of basins

Zones	N	AF	CI	HI	Bs	Smd	Sd	Dd	Dd1	Df	N1/N
Eastern	24	15.38	1.005	0.52	2.23	1.17	1.02	4.52	2.36	10.28	0.55
Central	28	11.84	1.46	0.49	2.16	1.22	1.56	2.93	1.52	8.43	0.40
Western	56	12.78	1.003	1.04	3.24	1.06	1.00	3.95	2.82	9.42	0.54

Table 2. Means of the morphometric properties related to the drainage basins in the northern and southern limbs of the anticline. N represents the number of basins

Zones	N	AF	CI	HI	Bs	Smd	Dd	Dd1	Df	N1/N
Northern	48	13.10	1.04	0.50	2.74	1.125	3.04	1.66	9.17	0.54
Southern	60	13.11	1.04	0.50	2.73	1.127	2.94	1.59	9.98	0.53

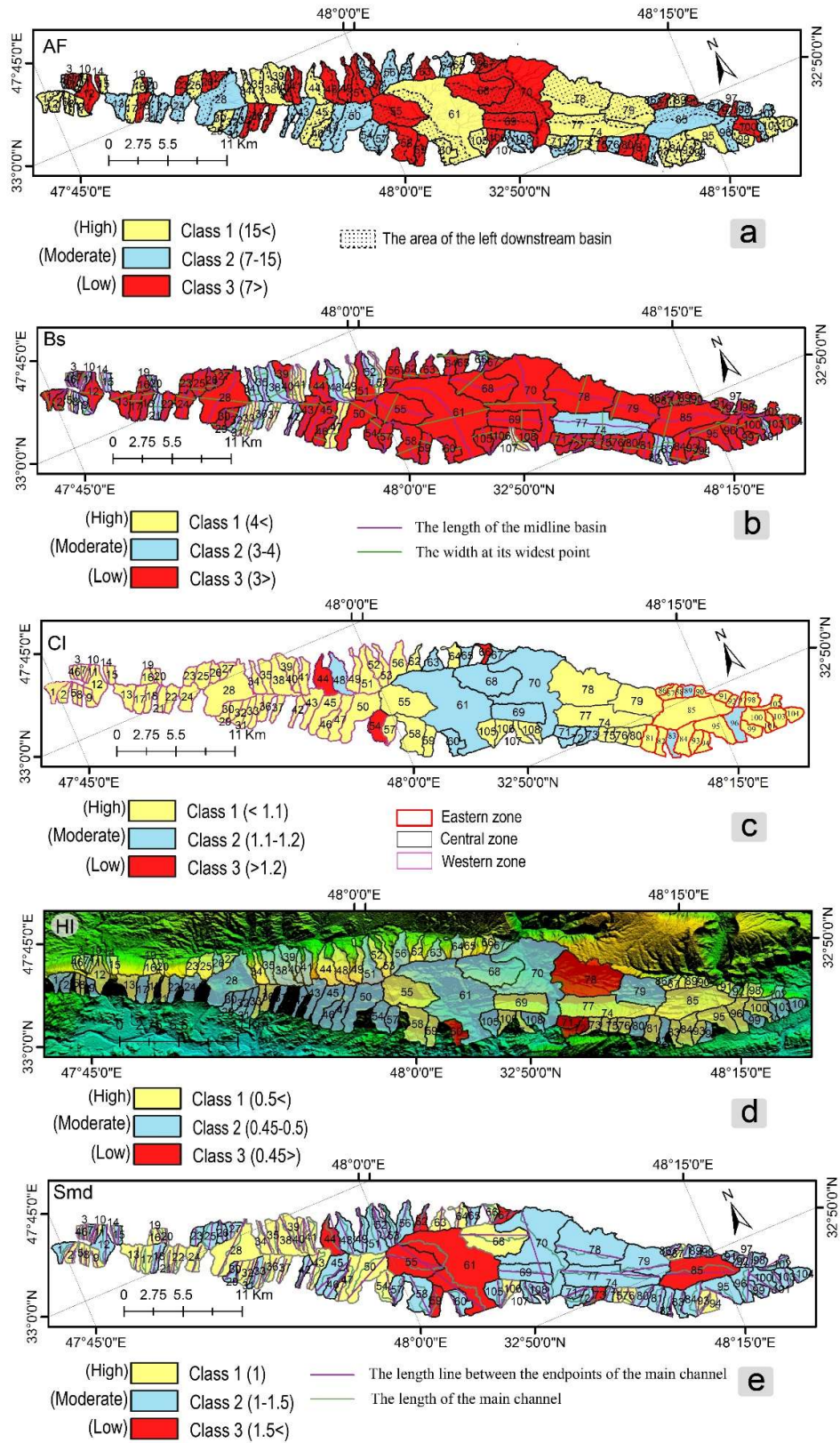


Figure 8. Spatial distribution maps of the geomorphologic indices in the study area. a) Asymmetry factor (AF). b) Drainage basin shape index (Bs). c) Crescentness index (CI). d) Hypsometric integral (HI). e) Main drainage sinuosity (Smd)

Based on the absolute values of AF, the basins in the eastern zone (15.38) had greater mean AF values than did those in the western and central zones (12.77 and 11.84, respectively). The mean sinuosity of the divide (Sd) of the basins in the central zone (1.56) is greater than that in the eastern and western zones (1.02 and 1.00, respectively). The values of Dd, Dd1, Df, and N1/N are greater in the western (3.95, 2.82, 9.42, and 0.54 respectively) and eastern zones (4.52, 2.36, 10.28, and 0.55, respectively) than in the central zone (2.93, 1.52, 8.43, and 0.40, respectively). The results of measuring the morphometric parameters related to the drainage basins in the northern and southern limbs are shown in Table 2. A comparison of these parameters for the northern and southern limbs reveals that the rates of tectonic activity and basin elongation are similar.

Discussion

Due to the variable rate of uplift and shortening in the Zagros orogenic belt (Vernant et al., 2004; Hessami et al., 2006), the development of folds related to active faults has led to changes in drainage morphometric parameters. Transient changes in the development of drainage patterns are influenced by the progressive growth of folds (Ramsey et al., 2008). Fold segmentation and lateral growth have profound significance for the structural history of the Zagros FTB, affecting hydrocarbon migration and the hydraulic connectivity and location of reservoirs (Ramsey et al., 2008).

The well-developed triangular facets of the straight mountain front along the frontal limb of the fold are the result of fault-related CH-Ant. These triangular facets confirm active faulting in the Quaternary (Silva, et al., 2003). The different elevations of these triangular facets indicate the process of tectonic reactivation and different stages of uplift (Koukouvelas, et al., 2021). In general, the development of wine-glass valleys and triangular facets in the frontal limb of the fold indicates a young topography with less erosion, implying lateral fold growth.

Three right-lateral strike-slip faults are exposed in the central part of the CH-Ant (F1, F2, and F3; Fig. 5b). F1 has cut the Amiran and Asmari Formations layers (Fig. 1b) and created fault scarps in the northern part of the study area (Fig. 5b). This also caused bending of the axis of CH-Ant (Fig. 5b). F2 and F3 caused displacement differences in the layers of the Asmari Formation, so the dip direction of the layers rotated from the southwest to the northeast. Overtaken forelimb beds in the central zone confirm differential lateral propagation of folding. These tear faults continue with a N–NW trend across the strike of the fold to accommodate the differential displacement between the two parts of the fold in the sedimentary cover. F4 is a part of the blind thrust related to CH-Ant, which is exposed on the surface of the Earth (Fig. 5b). Triangular surfaces with a dip of approximately 65 degrees have formed along this fault (Fig. 3c).

The size of the basins in the central area can be attributed to the activity of the faults, which causes the faults to deviate and join the drainages, and as a result, the basins are enlarged. According to the results obtained from geomorphic indices, some basins in the central part of the fold indicate high tectonic activity: AF (basins 60, 61, and 105), Bs (basin 107), CI (basins 64, 67, 68, 69, 105, 106, 107, and 108), HI (basins 65, 66, 69, 106 and 107), and Smd (basins 66, 68, and 106). The effects of the F1, F2, and F3 fault zones on increasing deformation and erosion and hence on increasing tectonic activity in these basins should not be ignored.

The folding geometry and changes in the hinge of the anticline control the shape of the basins. The meandering and deeply entrenched river around the eastern nose of CH-Ant confirms the lateral propagation of the fold. At the lowest topography of the anticline nose, the sinuosity of the river channel increases to maintain equilibrium (Ramsey et al., 2008). Fan-shaped tributary drainage channels with high junction angles connect to the main river on the fold nose, indicating lateral growth of the fold (Fig. 5c). The preservation of controlled tectonic

knickpoints along the river indicates that the river is still affected by uplift differences due to lateral propagation. Knickpoints are formed in the resistant limestone layers of the Asmari Formation. The large and relatively circular basins with high topographic slopes in the central zone (Fig. 4) represent the oldest part of the fold that has endured lateral and headward erosion. Basins with more elongation and less topographic slope are located in the eastern and western areas, which indicates a younger topography and less erosion.

In this research, the drainage networks were analyzed using morphometric indices (AF, HI, Bs, CI, Sd, Smd, Df, Dd, Dd1, and N1/N) to detect the lateral growth of CH-Ant. The results showed that the values of geomorphic parameters vary considerably in the three tectonic zones of the CH-Ant. The limbs in the central zone are characterized by larger basins with higher CI and Smd indices (Table 1), which indicates more erosion in this zone. In contrast, highly elongated, steeper slopes and younger basins (higher values of AF, HI, and Bs) with highly oriented drainage basins in the eastern and western zones indicate younger topography and less erosion. The analysis of the HI showed that the highest and lowest HIs were related to the western and central zones (Table 1), respectively, which indicates active lateral growth in the western zone.

A comparison of the morphometric characteristics of the drainage networks in the three tectonic zones revealed that the Dd, Dd1, and Df values are greater in the eastern and western zones than in the central zone (Table 1). These results indicate that more eroded parts of the CH-Ant (central zone) have lower Dd, Dd1 and Df than do the less eroded and younger parts (eastern and western zones) of the CH-Ant. The higher values of N1/N in the western and eastern parts can be attributed to the younger age of this area where drainages are not well developed with lower order streams compared to those in the central zone.

As the map in Fig. 7 shows, more basins are dominated by rock type 1 (75%<), whereas some CH-Ant basins are characterized by rock types 2 and 3, as 46 to 70% of these basins are composed of rock type 1 (strong). It is possible that all the geomorphic criteria of the fold are not evident due to the erosion of some geomorphic records of the growth of the lateral fold. More than 90% of the western zone consists of type 1 rocks. Therefore, the impact of lithology on geomorphic parameters is negligible. The lithology of intermediate to weak rocks leads to a decrease in HI and Bs, AF, CI, Dd, Dd1, Df, and N1/N values and an increase in CI, Smd, and Sd values in the central and eastern zones. The exposure of some soft rocks has facilitated lateral and vertical erosion. The graph in Fig. 10 shows the percentage distributions of morphometric indices (AF, Bs, Smd, HI, and CI) of rock types 1, 2 and 3 in classes 1, 2, and 3, respectively. The results show that nearly all classes (except class 3 Smd and HI) are dominated by type 1 (strong) bedrock.

Examining the mean values of geomorphic parameters in the northern and southern limbs showed similar results. These results show that the rate of lateral erosion in both limbs is almost the same. In many studies, river deflection has been identified as a crucial geomorphic indicator of the propagation of lateral folds (e.g., Ramsey et al., 2008; Bahrami et al., 2020; Bahrami and Stoke, 2023). Zhang et al. (2021) showed that from lateral growth to the merging of two folds, the eastern Qiolitage anticline formed in the southern Tian Shan piedmont. Numerical examinations of geomorphic indices have shown that inflected fold-crest topographic profiles with decreasing slopes and deflected rivers are valid evidence of the lateral growth of folds (Gao et al., 2023). The fold-crest profile shows a concave inflection from the central part toward the east and west, indicating the effect of lateral propagation in the plunges of the anticline (Fig. 8a). The number and location of slope breaks indicate the frequency and location of lateral propagation, respectively. Accordingly, I suggest that the CH-Ant propagates at least two times laterally.

River and runoff erosion activity is very evident in this area. Wind and water gaps are typical evidence of the evolution of drainage in the present-day landscape of CH-Ant. When the rate

of uplift is higher than the rate of incision, the height of the riverbed continues to rise, which eventually leads to the defeat and diversion of the river, and a wind gap is created. As seen in the eastern zone, when the uplift rate of the anticline becomes greater than the rate of river incision, the river breaks and diverts, leaving a wind gap (Wg1; Fig. 5c and 9). In the western zone, two wind gaps (Wg2 and Wg3) cut the entire width of the fold and are 1.45 and 3.77 km wide and up to 523 and 430 m deep, respectively (Figs. 5 and 9). The topographic profiles of Wg2 and Wg3 show that the western zone is uplifted in the middle parts of these valleys (Fig. 9b, c). Accordingly, the direction of water flow in the center of these valleys has been reversed. In the past, a river flowed from the south limb toward the north limb. The ongoing shortening and lateral growth of the fold caused the increasing uplift of the anticline. Over time, the direction of the water flow changed, and the rivers divided into two parts that flow in opposite directions.

These processes caused these wind gaps to appear in the western zone of CH-Ant. It is expected that in the future, these rivers will join parallel to the crest fold, bypass the western zone of the fold and finally connect to the nearby river. A cartoon model is prepared for the formation of wind gaps in CH-Ant over time (Fig. 11).

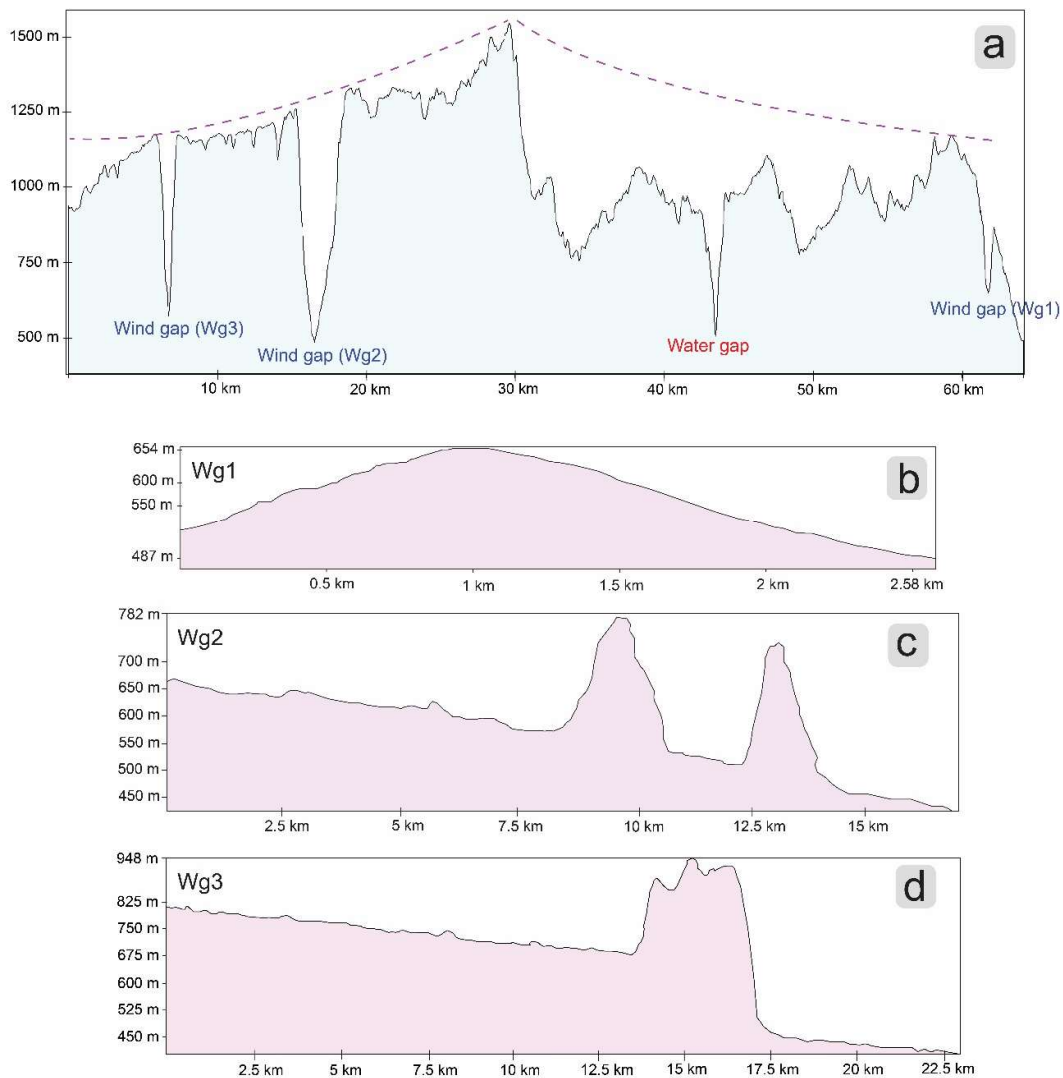


Figure 9. a) Longitudinal topographic profile along the crest of the Chenareh anticline. b, c, and d) Topographic profiles across the three wind gaps, locations given in Figure (5a; white lines). The profiles are perpendicular to the CH-Ant hinge line

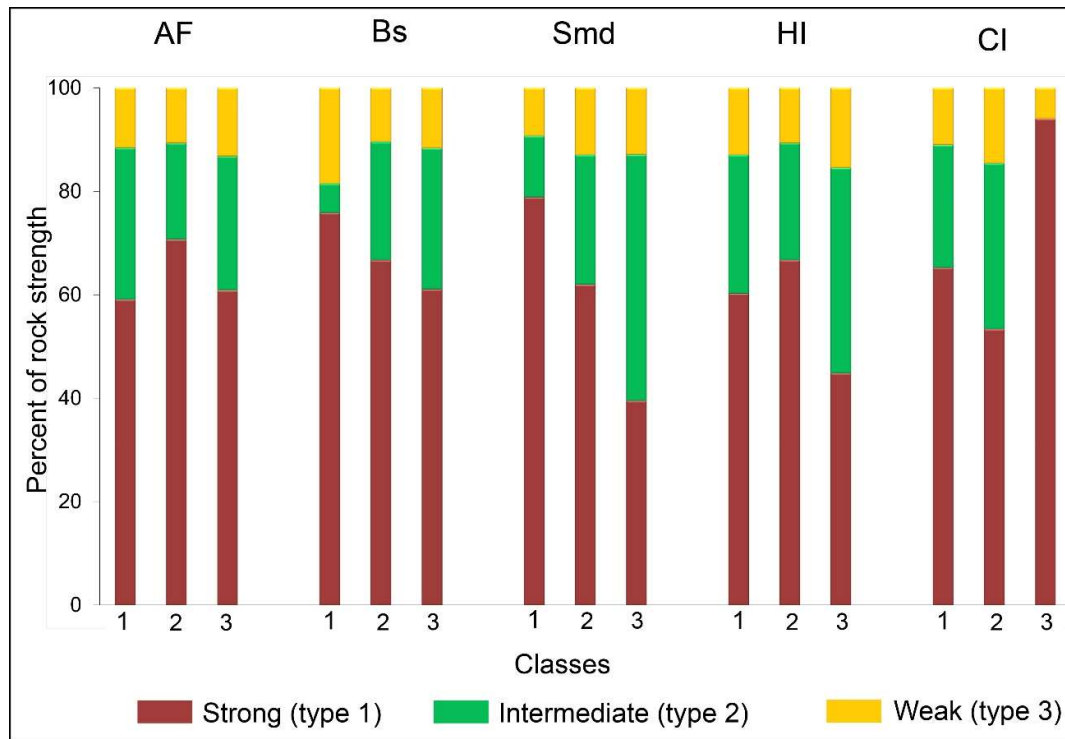


Figure 10. Distribution chart of morphometric parameters (CI, HI, Smd, Bs and AF) in different classes compared to the distribution percentage of the strength of rocks in the study area

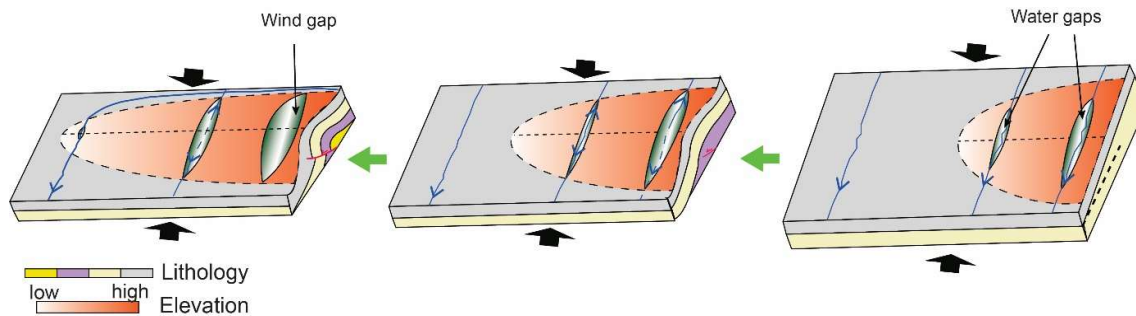


Figure 11. Cartoon showing the formation of the wind gap in the western and eastern zones of Chenareh anticline over time

The results of this study can aid in understanding the growth history of fault-related folds, understanding the accumulation and migration of hydrocarbons in the Zagros FTB, and identifying susceptible and vulnerable areas for effective disaster mitigation and management.

Conclusion

The Chenareh anticline (CH-Ant) in the Lorestan Province is located in the Zagros foreland fold-and-thrust belt (FTB). The style of deformation in the overlying sedimentary cover of the anticline is related to the activity of fault-related folds. In the study area, the basin shape, active tectonics and folded structural style control the drainage patterns of the basins. The lateral and vertical growth of the anticline plays an important role in the morphometry of the drainage basins. The morphometric parameters, including AF, HI, Bs, Smd, and CI, were estimated for 108 drainage basins. Additionally, the morphometric indices of the drainage networks (Df, Dd, Dd1, and N1/N) in the western, eastern, and central zones were calculated and compared. The

central zone was characterized by larger basins nearly parallel to the fold hinge; higher CI and Smd values; and lower mean AF, HI, and Bs values than the western and eastern zones. These results imply lower lateral erosion and younger topography in the western and eastern zones. The activity of strike-slip faults (F1, F2, and F3) in the central portion of the anticline has resulted in high tectonic activity in some basins according to the AF, CI, HI, and Smd parameters. Therefore, these faults have marked effects on increasing the mean values of these parameters. Nevertheless, the central zone had higher mean values of CI and Smd and lower values of HI and AF, than did the western and eastern zones. The drainage network indices Df, Dd, Dd1, and N1/N are the most useful indices for detecting the lateral propagation of CH-Ant. The higher values of Df, Dd, Dd1, and N1/N in the western and eastern noses of the anticline indicate that these parts are younger and laterally growing.

Geomorphic features and structural evidence in the study area include the following: 1) the dip of the fold limb decreases toward the west and east; 2) fan-shaped, curved tributary, parallel, and consequent drainage patterns develop on the eastern and western sides of the fold; 3) in the eastern and western zones of the CH-Ant, wind gaps appear in the Asmari Formation; 4) the relief of the topographic profile decreases from the crest of the fold toward the west and east; and 5) the sinuosity of the anticline divide (Sd) decreases from the core to the west and east of the fold. Geomorphological analyses, features and structural evidence confirm the development of lateral growth in the western and eastern zones of the CH-Ant.

Acknowledgments

The author thanks Professor Ali Kananian, Chief Editor of the Geopersia Journal for his editorial authority and constructive comments. I am grateful for the constructive comments of the anonymous reviewers, which helped to significantly improve the scientific content and presentation of the paper. The author would like to acknowledge the financial support of Lorestan University under grant number 1403403131405 for this research.

References

- Adeoti, B., Webb, A.A.G., 2022. Geomorphology of contractional salt tectonics along the Kuqa fold-thrust belt, northwestern China: Testing pre-kinematic diapir versus source-fed thrust and detachment fold models. *Journal of Structural Geology*, 161: 104638.
- Agard, P., Omrani, J., Jolivet, L., Mouthereau, F., 2005. Convergence history across Zagros (Iran): constraints from collisional and earlier deformation. *International journal of earth sciences*, 94: 401-419.
- Agard, P., Omrani, J., Jolivet, L., Whitechurch, H., Vrielynck, B., Spakman, W., Monié, P., Meyer, B., Wortel, R., 2011. Zagros orogeny: a subduction-dominated process. *Geological Magazine*, 148(5-6): 692-725.
- Alavi, M., 1994. Tectonics of the Zagros orogenic belt of Iran: new data and interpretations. *Tectonophysics*, 229(3-4): 211-238.
- Alipoor, R., Poorkermani, M., Zare, M., El Hamdouni, R., 2011. Active tectonic assessment around rudbar lorestan dam site, high zagros belt (SW of Iran). *Geomorphology*, 128(1-2): 1-14.
- Allen, M.B., Talebian, M., 2011. Structural variation along the Zagros and the nature of the Dezful Embayment. *Geological magazine*, 148(5-6): 911-924.
- Al-Saady, Y.I., Al-Suhail, Q.A., Al-Tawash, B.S., Othman, A.A., 2016. Drainage network extraction and morphometric analysis using remote sensing and GIS mapping techniques (Lesser Zab River Basin, Iraq and Iran). *Environmental Earth Sciences*, 75: 1-23.
- Azor, A., Keller, E.A., Yeats, R.S., 2002. Geomorphic indicators of active fold growth: South Mountain–Oak Ridge anticline, Ventura basin, southern California. *Geological society of america bulletin*, 114(6): 745-753.
- Bahrami, S., 2013. Analyzing the drainage system anomaly of Zagros basins: Implications for active

- tectonics. *Tectonophysics*, 608: 914-928.
- Bahrami, S., Stokes, M., 2023. Analyzing drainage basin orientation and its relationship to active fold growth (Handun anticline, Zagros, Iran). *Geomorphology*, 426: 108605.
- Bahrami, S., Capolongo, D., Mofrad, M.R., 2020. Morphometry of drainage basins and stream networks as an indicator of active fold growth (Gorm anticline, Fars Province, Iran). *Geomorphology*, 355: 107086.
- Bahrami, S., Ehteshami-Moinabadi, M., Tuyserkani, M.S., 2024. Quantitative evaluation of morphometric parameters of drainage system in the forelimb and backlimb of the Asmari Anticline, Zagros, Iran. *Journal of Structural Geology*, 184: 105151.
- Bahroudi, A., Koyi, H.A., 2004. Tectono-sedimentary framework of the Gachsaran Formation in the Zagros foreland basin. *Marine and Petroleum Geology*, 21(10): 1295-1310.
- Bretis, B., Bartl, N., Grasmann, B., 2011. Lateral fold growth and linkage in the Zagros fold and thrust belt (Kurdistan, NE Iraq). *Basin Research*, 23(6): 615-630.
- Borne, J.A., Twidale, C.R., 2011. Neglected and cryptostructural effects in drainage development.
- Bufe, A., Paola, C., Burbank, D.W., 2016. Fluvial bevelling of topography controlled by lateral channel mobility and uplift rate. *Nature Geoscience*, 9(9): 706-710.
- Burberry, C.M., Cosgrove, J.W., Liu, J.G., 2008. Spatial arrangement of fold types in the Zagros Simply Folded Belt, Iran, indicated by landform morphology and drainage pattern characteristics. *Journal of Maps*, 4(1): 417-430.
- Burberry, C.M., Cosgrove, J.W., Liu, J.G., 2010. A study of fold characteristics and deformation style using the evolution of the land surface: Zagros Simply Folded Belt, Iran. *Geological Society, London, Special Publications*, 330(1): 139-154.
- Carruba, S., Perotti, C.R., Buonaguro, R., Calabrò, R., Carpi, R., Naini, M., 2006. Structural pattern of the Zagros fold-and-thrust belt in the Dezful Embayment (SW Iran).
- Collignon, M., Yamato, P., Castelltort, S., Kaus, B.J., 2016. Modeling of wind gap formation and development of sedimentary basins during fold growth: application to the Zagros Fold Belt, Iran. *Earth Surface Processes and Landforms*, 41(11): 1521-1535.
- Devi, R.M., Bhakuni, S.S., Bora, P.K., 2011. Tectonic implication of drainage set-up in the Sub-Himalaya: a case study of Papumpare district, Arunachal Himalaya, India. *Geomorphology*, 127(1-2): 14-31.
- Elyasi, A., Goshtasbi, K., 2015. Using different rock failure criteria in wellbore stability analysis. *Geomechanics for Energy and the Environment*, 2: 15-21.
- Elyasi, A., Goshtasbi, K., Saeidi, O., Torabi, S.R., 2014. Stress determination and geomechanical stability analysis of an oil well of Iran. *Sadhana*, 39: 207-220.
- Gao, L., He, C., Rao, G., Yang, C.J., Yuan, X., Lai, J., Tang, P., Wu, L., 2023. Numerical examination of the geomorphic indicators for lateral fold growth. *Geomorphology*, 432: 108702.
- Hajialibeigi, H., 2011. Signatures of the Balarud Deep Seated Fault Zone in Khushab Anticline, SW Iran, An Integrated Study. *Journal of Sciences, Islamic Republic of Iran*, 22(1): 33-81.
- He, C., Rao, G., Yang, R., Hu, J., Yao, Q., Yang, C.J., 2019. Divide migration in response to asymmetric uplift: Insights from the Wula Shan horst, North China. *Geomorphology*, 339: 44-57.
- Hessami, K., Koyi, H.A., Talbot, C.J., Tabasi, H., Shabaniyan, E., 2001. Progressive unconformities within an evolving foreland fold-thrust belt, Zagros Mountains. *Journal of the Geological Society*, 158(6): 969-981.
- Hessami, K., Nilforoushan, F., Talbot, C.J., 2006. Active deformation within the Zagros Mountains deduced from GPS measurements. *Journal of the Geological Society*, 163(1): 143-148.
- Horton, R.E., 1932. Drainage basin characteristics. *Trans. Am. Geophys. Union* 13, 350-361.
- Hubbard, J., Shaw, J.H., 2009. Uplift of the Longmen Shan and Tibetan plateau, and the 2008 Wenchuan (M= 7.9) earthquake. *Nature*, 458(7235): 194-197.
- Keller, E.A., Gurrola, L., Tierney, T.E., 1999. Geomorphic criteria to determine direction of lateral propagation of reverse faulting and folding. *Geology*, 27(6): 515-518.
- Keller, E., Pinter, N., 2002. *Active Tectonics: Earthquakes, Uplift, and Landscape*. Prentice Hall, New Jersey.
- Koukouvelas, I.K., Nikolakopoulos, K.G., Kyriou, A., Caputo, R., Belesis, A., Zygouri, V., Verroios, S., Apostolopoulos, D., Tsentzos, I., 2021. The March 2021 Damasi earthquake sequence, central Greece: Reactivation evidence across the westward propagating Tyrnavos graben. *Geosciences*,

- 11(8): 328.
- Lavé, J., Avouac, J.P., 2000. Active folding of fluvial terraces across the Siwaliks Hills, Himalayas of central Nepal. *Journal of Geophysical Research: Solid Earth*, 105(B3): 5735-5770.
- Liffner, J.W., Hewa, G.A., Peel, M.C., 2018. The sensitivity of catchment hypsometry and hypsometric properties to DEM resolution and polynomial order. *Geomorphology*, 309: 112-120.
- Lu, R., He, D., Xu, X., Wang, X., Tan, X., Wu, X., 2018. Seismotectonics of the 2016 M 6.2 Hutubi earthquake: Implications for the 1906 M 7.7 Manas earthquake in the northern Tian Shan belt, China. *Seismological Research Letters*, 89(1): 13-21.
- Machuca, S., García-Delgado, H., Velandia, F., 2021. Studying active fault-related folding on tectonically inverted orogens: A case study at the Yariguíes Range in the Colombian Northern Andes. *Geomorphology*, 375: 107515.
- McClay, K.R., Whitehouse, P.S., Dooley, T., Richards, M., 2004. 3D evolution of fold and thrust belts formed by oblique convergence. *Marine and Petroleum Geology*, 21(7): 857-877.
- McClusky, S., Reilinger, R., Mahmoud, S.B.S.D., Ben Sari, D., Tealeb, A., 2003. GPS constraints on Africa (Nubia) and Arabia plate motions. *Geophysical Journal International*, 155(1): 126-138.
- Melosh, B.L., Keller, E.A., 2013. Effects of active folding and reverse faulting on stream channel evolution, Santa Barbara Fold Belt, California. *Geomorphology*, 186: 119-135.
- Mukherjee, S., 2015. A review on out-of-sequence deformation in the Himalaya. *Special Publications*, 412(1): 67-109.
- Mukherjee, S., Carosi, R., van der Beek, P., Mukherjee, B.K., Robinson, D.M., 2015. Tectonics of the Himalaya: an introduction. *Special Publications*, 412(1): 1-3.
- Mukherjee, S., Mukherjee, B.K., Thiede, R.C., 2013. Geosciences of the Himalaya–Karakoram–Tibet orogen. *International Journal of Earth Sciences*, 102: 1757-1758.
- Mumipour, M., Nejad, H.T., 2011. Tectonics Geomorphology Setting of Khayiz Anticline derived from GIS processing, Zagros Mountains, Iran. *Asian Journal of Earth Sciences*, 4(3), p.171.
- Nag, S.K., Chakraborty, S., 2003. Influence of rock types and structures in the development of drainage network in hard rock area. *Journal of the Indian Society of Remote Sensing*, 31: 25-35.
- Obaid, A.K., Allen, M.B., 2017. Landscape maturity, fold growth sequence and structural style in the Kirkuk Embayment of the Zagros, northern Iraq. *Tectonophysics*, 717: 27-40.
- Pash, R.R., Davoodi, Z., Mukherjee, S., Dehsarvi, L.H., Ghasemi-Rozveh, T., 2021. Interpretation of aeromagnetic data to detect the deep-seated basement faults in fold thrust belts: NW part of the petroliferous Fars province, Zagros belt, Iran. *Marine and Petroleum Geology*, 133, p.105292.
- Pavano, F., Catalano, S., Romagnoli, G., Tortorici, G., 2018. Hypsometry and relief analysis of the southern termination of the Calabrian arc, NE-Sicily (southern Italy). *Geomorphology*, 304: 74-88.
- Peyrowan, H.R., Shariat Jafari, M., 2013. Presentation of a comprehensive method for determining erodibility rate of rock units with a review on Iranian geology. *Watershed Engineering and Management*, 5(3): 199-213.
- Ramírez-Herrera, M.T., 1998. Geomorphic assessment of active tectonics in the Acambay Graben, Mexican volcanic belt. *Earth Surface Processes and Landforms: The journal of the British Geomorphological Group*, 23(4): 317-332.
- Ramkumar, M., Santosh, M., Rahaman, S.M.A., Balasundareswaran, A., Balasubramani, K., Mathew, M.J., Sautter, B., Siddiqui, N., Usha, K.P., Sreerhishya, K., Prithiviraj, G., 2019. Tectonomorphological evolution of the Cauvery, Vaigai, and Thamirabarani River basins: Implications on timing, stratigraphic markers, relative roles of intrinsic and extrinsic factors, and transience of Southern Indian landscape. *Geological Journal*, 54(5): 2870-2911.
- Ramsey, L.A., Walker, R.T., Jackson, J., 2008. Fold evolution and drainage development in the Zagros mountains of Fars province, SE Iran. *Basin Research*, 20(1): 23-48.
- Sarkarinejad, K., Goftari, F., 2019. Thick-skinned and thin-skinned tectonics of the Zagros orogen, Iran: constraints from structural, microstructural and kinematics analyses. *Journal of Asian Earth Sciences*, 170: 249-273.
- Sepehr, A., Honarmandnejad, S., 2012. Actual soil erosion risk mapping using modified CORINE method (Case study: Jahrom basin). *Journal of Geography and Environmental Hazards*, 1(3): 57-72.
- Silva, P.G., Goy, J.L., Zazo, C., Bardaji, T., 2003. Fault-generated mountain fronts in southeast Spain: geomorphologic assessment of tectonic and seismic activity. *Geomorphology*, 50(1-3): 203-225.

- Sissakian, V.K., Elias, Z., Al-Ansari, N., 2019. Deducing the lateral growth of anticlines using drainage analysis and geomorphological features. *Geotectonics*, 53: 140-154.
- Stokes, M., Mather, A.E., 2015. Controls on modern tributary-junction alluvial fan occurrence and morphology: High Atlas Mountains, Morocco. *Geomorphology*, 248: 344-362.
- Strahler, A.N., 1952. Hypsometric (area-altitude) analysis of erosional topography. *Geological society of America bulletin*, 63(11): 1117-1142.
- Talebian, M., Jackson, J., 2002. Offset on the Main Recent Fault of NW Iran and implications for the late Cenozoic tectonics of the Arabia–Eurasia collision zone. *Geophysical Journal International*, 150(2): 422-439.
- Vernant, P., Nilforoushan, F., Hatzfeld, D., Abbassi, M.R., Vigny, C., Masson, F., Nankali, H., Martinod, J., Ashtiani, A., Bayer, R., Tavakoli, F., 2004. Present-day crustal deformation and plate kinematics in the Middle East constrained by GPS measurements in Iran and northern Oman. *Geophysical Journal International*, 157(1): 381-398.
- Walcott, R.C., Summerfield, M.A., 2008. Scale dependence of hypsometric integrals: an analysis of southeast African basins. *Geomorphology*, 96(1-2): 174-186.
- Walker, R.T., Ramsey, L.A., Jackson, J., 2011. Geomorphic evidence for ancestral drainage patterns in the Zagros Simple Folded Zone and growth of the Iranian plateau. *Geological Magazine*, 148(5-6): 901-910.
- Woodbridge, K.P., Pirasteh, S., Parsons, D.R., 2019. Investigating fold-river interactions for major rivers using a scheme of remotely sensed characteristics of river and fold geomorphology. *Remote Sensing*, 11(17), p.2037.
- Xu, X., Wen, X., Yu, G., Chen, G., Klinger, Y., Hubbard, J., Shaw, J., 2009. Coseismic reverse-and oblique-slip surface faulting generated by the 2008 Mw 7.9 Wenchuan earthquake, China. *Geology*, 37(6): 515-518.
- Zarei, S., Faghih, A., Keshavarz, S., Zarei, E., 2023. Growth history and linkage pattern of fault-related folds deciphered from geomorphic analysis: A case study from the Dalan Anticline, Zagros Mountains, SW Iran. *Journal of African Earth Sciences*, 202, p.104927.
- Zarei, E., Faghih, A., Soleimani, M., Zarei, S., 2024. Assessment of relative tectonic activity in the Lar region, Zagros Fold-Thrust Belt, SW Iran: Insights from geomorphometric analysis. *Earth Surface Processes and Landforms*, 49(3): 1199-1213.
- Zebari, M.M., Burberry, C.M., 2015. 4-D evolution of anticlines and implications for hydrocarbon exploration within the Zagros Fold-Thrust Belt, Kurdistan Region, Iraq.
- Zielke, O., Arrowsmith, J.R., Ludwig, L.G., Akçiz, S.O., 2010. Slip in the 1857 and earlier large earthquakes along the Carrizo Plain, San Andreas fault. *science*, 327(5969): 1119-1122.

